http://dx.doi.org/10.21611/qirt.1992.029

Time-resolved pulsed stimulated infrared thermography applied to carbon-epoxy non destructive evaluation

by J.-C. KRAPEZ, D. BOSCHER, Ph. DELPECH, A. DEOM
G. GARDETTE, and D. BALAGEAS

Thermophysics Division, ONERA , BP 72, F-92322 CHATILLON-Cedex, France.

Abstract

Since several years, time-resolved pulsed stimulated infrared thermography (SIRT) has been developed at ONERA with the aim of combining fast screening and quantitative characterization. The analysis of pixel by pixel thermograms leads to depth-location and thermal resistance images of delaminations. In this paper we present recent enhancements of the portable SIRT system and refinement of the data reduction procedure which demonstrate the possibility of detecting and evaluating delaminations in C-epoxy at depths higher than 3mm. A 2-D inversion procedure is proposed to better characterize defects of reduced lateral extend as compared to the former 1-D method.

Nomenclature

l, l_1, d, d_{app} sample thickness; defect depth; real and apparent lateral size of the defect (m)
$d^* = d/l_1(a_z/a_r)^{1/2}$ and $d_{app}' = d_{app}/l(a_z/a_r)^{1/2}$
$l_2 = l\text{-}l_1$ and its non-dimensional counterpart $l_2^* = l_2/l_1$
R_1 defect's resistance ($W^{-1}.m^2.K$), and its non-dimensional counterpart $R_1^* = R_1 k_z/l_1$
a_r, a_z in-plane and axial diffusivities of the sample ($m^2.s^{-1}$)
k_z axial conductivity ($W.m^{-1}.K^{-1}$)
h heat loss coefficient ($W.m^{-2}.K^{-1}$), and Biot number $h^* = hl_1/k_z$
T, T_{ref} front face temperature over the center of a defect and over a defect-free region (K)
$Cr = 100(1\text{-}T/T_{ref})$ relative contrast (%)
t time (s), and Fourier number { $Fo = a_z t/l^2$ }; Fo^* is expressed relatively to l_1

1. Introduction

Pulsed photothermal nondestructive testing has been applied to the characterization of delaminations in carbon-epoxy laminates and some results were already presented [1-3]. A data reduction software developed using the correlations presented in [2] yields images graduated in location depth and thermal resistance (or equivalent air gap thickness) of the defects [3]. They were in good agreement with the known structure of the sample but the defects deeper than 2 mm in the carbon/epoxy were difficult to detect. In this paper we present recent improvements in the stimulated infrared thermography system and in the software (better normalization of the thermal images) which allow marked enhancement of the detection.

The depth and resistance images shown in [3] were obtained through the application of a defect identification algorithm assuming a 1-D heat transfer through the material [2]. Such an hypothesis becomes less and less true as the lateral dimension to depth ratio of the defect decreases. A data reduction assuming a 2-D heat transfer will here be described. The defect characteristics as obtained by both approaches will be compared and some criteria will be proposed to help for the choice between these methods.

http://dx.doi.org/10.21611/qirt.1992.029

2. The problem of normalization in pulsed stimulated infrared thermography

The purpose of normalization is to clear IR images of the artefacts due to the possible non uniformity of the heat flux or of the optical properties. Its principle consists in dividing every image by a reference image (or the sum of a series of images), pixel by pixel [4]. The reference image is taken during the very beginning of the cooling phase which follows the pulsed heat deposition, i.e. at a moment when the surface temperature of the sample is not yet affected by the presence of the internal defects and when the spurious reflections of the radiating source on the sample have disappeared. Such a simple normalization proves however to be inefficient for samples containing defects whose depth covers a large range. Indeed, in order to detect the deepest defects without overheating the specimen it is necessary to use rather long pulses with reduced power. In that case the shallowest defects may perturb the surface temperature too early, possibly already during the heating.

The remedy could consist in making two tests, one with a very short pulse to obtain reference image(s) and, a second one with a longer pulse duration for defects characterization. However, the relatively low refreshment frequency of classical IR cameras is the limiting factor which may prevent from obtaining a correct reference (for rapidly evolving thermal fields, the non-
96 isochronicity of the camera can too strongly affect the images aspect).

One could also use an other specimen (the reference sample), assumed to be identical to the first one, but without defects. Nevertheless, in some cases it is impossible to find such a sample and, furthermore the so-obtained normalization would only correct for the non uniformity of the incident radiation, not for the possible space variability of the optical properties.

An alternative consists in taking a reference image(s) at the end of the test, when the thermal contrasts induced by the defects have become very weak, but at this moment the 3-D heat diffusion has already smoothed the pattern induced by the high spatial frequency variations of the optical properties. Furthermore, in the case of anisotropic materials, with in-plane conductivity much higher than through-plane conductivity (i.e. carbon-epoxy composite materials) even the low frequency non-uniformity of the heat flux can be smoothed. Yet, this late normalization (let us call it type II normalization as opposed to the early images normalization that we shall call type I normalization) can partly correct the effects of the free convection which develops at longer times. In fact, type I normalization gives good results in the areas under which are the deep defects and type II normalization in the areas where near-surface defects are present.

These considerations are illustrated by the results obtained with the 5mm-thick carbon-epoxy sample already used in [1-4], which contains 80 µm-thick square and rectangular Teflon implants at various depths. The Cedip-ONERA PTR 9010® system used was previously described [2, 5]. The time duration of the pulse for the present tests is 2 s and the total time of the measurement is 35 s. *Figure 1* presents the thermal resistance image obtained using type I normalization and the algorithm of [2] which assumes 1-D heat transfer in an adiabatic semi-infinite material. *Figure 2* gives the same results with type II normalization. It is obvious that the near-surface defects are more visible on the type II normalized image and the deeper defects more visible on the type I normalized image. In fact, by normalizing at a given pixel by a temperature value corresponding to times when a possible contrast has either already appeared or not yet disappeared, one obtains a reduced value for the resistance. We therefore constructed a synthetic image by choosing, pixel by pixel, the normalization leading to the highest resistance. Then a noise reduction procedure was applied by which no defect was assumed at a given pixel if it has less than 3 neighbours revealing a defect. The resulting resistance image and the corresponding depth map are given on *color plates A*and B.* Defects of lateral size 20x20 and 10x10 mm and at a depth ranging from 0.3 to 3.75 mm are clearly revealed.

However, the resistance map proves to be particularly affected by the lateral heat diffusion effects: the calculated depth is nearly uniform over the implants, the resistance is, on the contrary, bell-shaped. As the lateral size to depth ratio of the defect gets lower even the resistance value identified at the central pixel may be perturbed by the side effects. A multi-dimensional approach is thus necessary for a more precise characterization.

* *The colour plates of this article* **29** *are located on page* **IX** *of the colour gathering, at the end of the book*

http://dx.doi.org/10.21611/qirt.1992.029

3. Defect evaluation by 2-D inversion

3.1 Presentation of the inversion method

We performed on the aforementioned IR images a 2-D data inversion procedure which was already described [6, 7] and whose salient features will now be reviewed .

Two routines were developed for the characterization of delaminations and flat bottom holes in anisotropic plates. Axial as well as planar symmetries were considered, i.e. penny-shaped and ribbon-like delaminations on one hand and cylindrical holes and slots on the other hand. In order to simulate at best the actual conditions, convection was also taken into account in the model.

For the resolution of the direct problem of heat transfer we chose a 2-D finite difference model with the Control Volume approach for the spatial discretization and ADI procedure for the temporal progression. The use of non-uniform spatial and temporal grids provided increased precision for the numerical results. Starting from the knowledge of the defect normalized depth l_2^* and lateral size d^*, those grids are automatically generated. Given the values of R_1^* and h^* (relative resistance and Biot number) the thermal field evolution following the absorption of a short pulse at the front surface is then computed, and thus the evolution of the front surface relative contrast and its peculiarities (maximum Cr_{max}, its occurrence Fo_{max}, its half-rise time $Fo_{1/2}^-$, and half-drop time $Fo_{1/2}^+$, the position of the steepest gradient at Fo_{max} was chosen to define the apparent lateral size of the subsurface defect: d_{app}).

An example of a direct problem solution is given in *figures 3* and *4*. The defect corresponds to a 100 µm-thick air layer with a normalized diameter d^* of 2.4 at 1 mm depth in a 3.4 mm graphite-epoxy laminate submitted to natural convection. *Figure 3* shows part of the temperature distribution at Fo_{max} within the sheet. In *figure 4* the relative temperature contrast across the irradiated surface is plotted for different values of the Fourier number.

Typical computer times for a given geometrical configuration varied from nearly 10 to 100 seconds. Such durations are relatively long for inclusion in an inverse-problem iterative routine. A large number of direct finite difference computations were thus performed once for all to constitute a data bank of Cr_{max}, $Fo^*_{1/2}{}^-$, $Fo^*_{1/2}{}^+$, and d_{app}/d values which will next be interpolated in the actual inversion process (6540 different combinations of the normalized variables: l_2^*, R_1^*, d^*, and h^* were considered).

A few representative results, showing the variations of Cr_{max} with the defect thermal resistance and geometry are shown in *figure 5*. An abacus connecting $Fo^*_{1/2}{}^-$ with Cr_{max} can also be constructed *(figure 6)*. These families of curves are the fellows for 2-D diffusion of the correlation curves once presented for the 1-D case [1].

Bundle of curves were also obtained for $Fo^*_{1/2}{}^+$ and d_{app}/d and presented in [7]. It should be noted that for d^*>1.5 (narrower defects are hardly detectable), the apparent defect size d_{app} measurement gives an estimation with less than 20% error of the actual size. Taking finally d_{app} as a good estimation of d, the measurement of the maximum contrast and its half-rise time, allows, by an iterative use of the abacuses on *figure 5* and *figure 6*, the depth and resistance of the delamination to be determined, knowing the thermophysical properties of the host material. However, because these abacus only pertain to the spetial case of a thick adiabatic plate, we preferred, for a general approach, to rely on a multidimensional interpolation of the Cr_{max}, $Fo^*_{1/2}{}^-$, $Fo^*_{1/2}{}^+$, and d_{app}/d *vs.* l_2^*, d^*, and R_1^* functions for the 9 different values between 0. and 1 that we considered for the convective Biot number h^*.

The data inversion is based on the non-linear minimization of the following functional defined as the square difference between computed and experimental parameters (four parameters are considered for the determination of the four unknowns l_2^*, R_1^* , d^*, and h^*):

$$\chi^2\left(l_2^*, d^*, R_1^*, h^*\right) = \left(\frac{Cr_{max}}{Cr_{max}|_{exp}} - 1\right)^2 + \left(\frac{Fo_{1/2^-}}{Fo_{1/2^-}|_{exp}} - 1\right)^2 + \left(\frac{d_{app}{}'}{d_{app}|_{exp}{}'} - 1\right)^2 + \left(\frac{Fo_{1/2^+}}{Fo_{1/2^+}|_{exp}} - 1\right)^2 \qquad (1)$$

http://dx.doi.org/10.21611/qirt.1992.029

The nonlinear least-square problem is solved using a modified Levenberg-Marquardt method which relies on 3-D B-splines interpolations which were previously performed for the reduced parameters Cr_{max}, $Fo^*_{1/2^-}$, $Fo^*_{1/2^+}$, and d_{app}/d on grids as partially illustrated on *figure 5*. The tensor-product B-splines coefficients were computed once for all and stored in nine different files from which the proper one is read before a particular minimization process. This results in execution times of the order of 1s for a single minimization. If the heat loss coefficient h is considered as unknown, several such minimizations have to be done until the smallest χ^2 value is found. A complete inversion therefore requires about 5s.

We refer the reader to [6, 7] for an analysis of the performances of this particular inversion routine. Several defect configurations which didn't participate to the interpolant construction were used for direct calculations whose results were injected as input for the inversion process. The depth and lateral size of the delamination were retrieved with errors less than 2%, whereas for its resistance the error didn't exceed 10% as long as $R_1^*/d^*<5$. These tests on pseudo-experimental values confirmed the intuitive result that the resistance of a delamination will be all the less well characterized that it is high (saturation effect) and the defect extend is low (lateral diffusion effect predominance).

98

3.2 Comparison of the 1-D and 2-D inversion results

As far as the 1-D approach is concerned the inversion is performed on each pixel as if the underlying thermal barrier was infinite in extend. Depth and resistance maps can thus be constructed, even though the values at the pixels above the defects borders are of questionable significance. On the other hand, the 2-D approach allows to retrieve unique values for the depth and the resistance of a detected defect. This one is assumed to be circular or very elongated, to be parallel to the surface, and to present an uniform resistance (because the diffuse nature of thermal waves tends to obliterate the effects of small irregularities in the defect geometry, a 2-D *disk-like* modelization of the *square* Teflon® implants is thought to give acceptable results).

We plotted on *figure 7* the air gap thickness equivalent to the defect resistance as obtained through the application of the 1-D (identification at the center of the defect) and the 2-D procedures. One can notice that the 1-D identified resistance decreases with the defect relative extend d^*, whereas such trend is not observed for the 2-D values. The underestimation of the resistance as provided by the 1-D method ranges from 10% for $d^*=6$ to more than 60% for $d^*=1.5$. The fact that heat passes round the internal defects has thus to be taken into account for their resistance calculation as soon as d^* is lower than about 5.

No substantial difference is however found between the two methods in regard to the identified depth of the implants *(figure 8)*. In both cases this parameter is all the more underestimated as is grows. The depth of defects located at or beyond the middle plane of the sample proves difficult to be evaluated precisely (one should nevertheless mention that the implant located at 3.75mm under the surface was partly covered by an other implant at 1.25mm whose presence is thought to perturb the depth characterization of the former).

4. Conclusion

Some impediments existed for pulsed thermography to become a more precise quantitative tool for NDE. These originated first from the unavoidable lack of homogeneity concerning the heating flux and the sample optical properties, and then from the multidimensional aspect of heat diffusion which handicaps the analysis of deep and narrow defects.

Substantial enhancement of the defect detection and characterization was obtained owing to a normalization made with both early and late images, providing afterwards synthetic maps of the depth and resistance of the subsurface anomalies.

A 2-D inversion routine was developed in order to remedy the shortcomings shown by the simpler 1-D inversion when applied to deep and little extended defects. Inferred values for the thermal resistance were found higher and less scattered with the 2-D approach.

http://dx.doi.org/10.21611/qirt.1992.029

Combined together, the new normalization process and the 2-D inversion routine constitute a marked step for *pulsed thermography* in its evolution towards a *precise NDE tool.*

Acknowledgement

The 2-D inversion procedure was developed by J.-C. Krapez when he was at Industrial Material Institute (NRC Canada) to which we are indebted for the software lending.

REFERENCES

[1] BALAGEAS (D.L.), DEOM (A.A.) and BOSCHER (D.M.). - *Characterization and NDT of Carbon-Epoxy Composites by a Pulsed Phothermal Method* - Materials Evaluations, *45*, 1987, p. 461-465.

[2] DEOM (A.A.), BOSCHER (D.M.) and BALAGEAS (D.L.) - *Pulsed photothermal non destructive testing. Application to carbon epoxy laminates.* Review of Progress in Quantitative NDE, edited by D.O. Thompson and D.E. Chimenti (Plenum Press, New-York, 1990), Vol. 9A, p. 525-531.

[3] BALAGEAS (D.L.), DELPECH (Ph.), BOSCHER (D.M.) and DEOM (A.A). - *New developments in stimulated infrared thermography applied to non destructive evaluation of laminates.* Review of Progress in Quantitative NDE, 1991, Vol. 10B, p. 1073-1081.

[4] BALAGEAS (D.L.), BOSCHER (D.M.) and DEOM (A.A.). - *Temporal moment method in pulsed photothermal radiometry: application to carbon epoxy NDT.* Photoacoustic and Photothermal Phenomena, edited by P. Hess and J. Pelzl (Springer-Verlag, 1988), p. 500-502.

[5] POTET (P.), BALAGEAS (D.L.), DEOM (A.A.) and BOSCHER (D.M.).- *The PTR 8900: an industrial apparatus for testing materials by infrared photothermography.* Review of Progress in Quantitative NDE, 1990, Vol. 9A, p. 1017-1023.

[6] KRAPEZ (J.-C.). - *Contribution a la caractérisation des défauts de type délaminage ou cavité par thermographie stimulée.* Doctoral Thesis, Ecole Centrale de Paris, Châtenay-Malabry (1991).

[7] KRAPEZ (J.-C.), MALDAGUE (X.) and CIELO (P.). - *Thermographic nondestructive evaluation: data inversion procedures.* Research in Nondestructive Evaluation, 3 , 1991, p. 81-124.

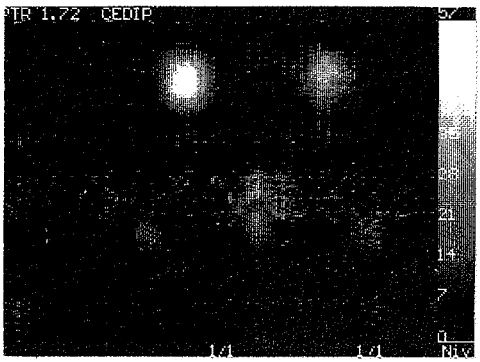

Fig.1. - Resistance image using type I normalization and 1-D inversion algorithm.

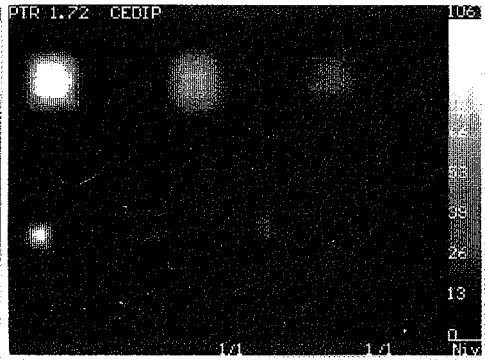

Fig.2. - Same with type II normalization (in μm for the equivalent air gap)

http://dx.doi.org/10.21611/qirt.1992.029

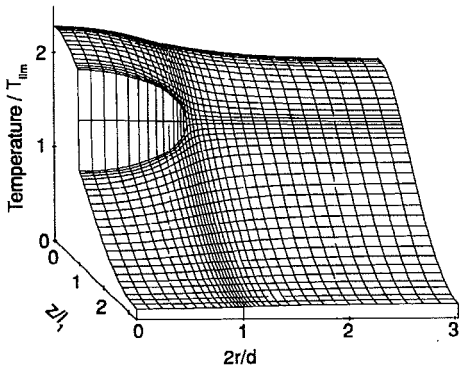

Fig.3. - Plot of the temperature distribution computed by the finite difference model (see text)

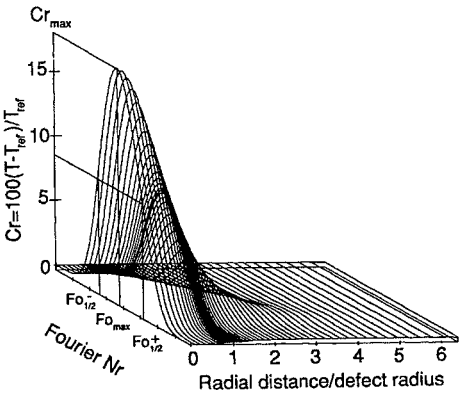

Fig. 4. - Plot of the relative contrast vs. time and radial distance along the surface

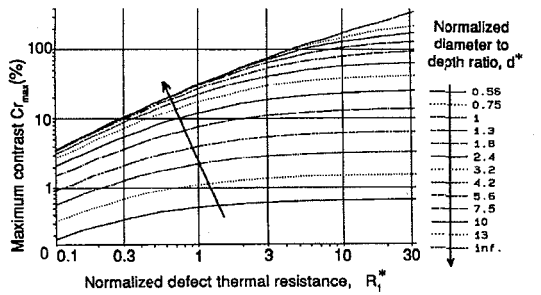

Fig. 5. - Correlation between Cr_{max}, $R_1{}^*$, and d^*

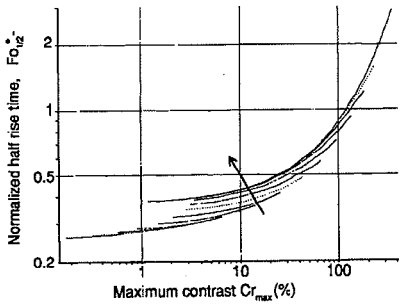

Fig. 6. - Same between Cr_{max}, $Fo^*{}_{1/2}$, and d^*

(disk-type delamination at a depth much smaller than the sheet thickness ($l_1/l_2 = 0.1$) and in the absence of surface heat losses)

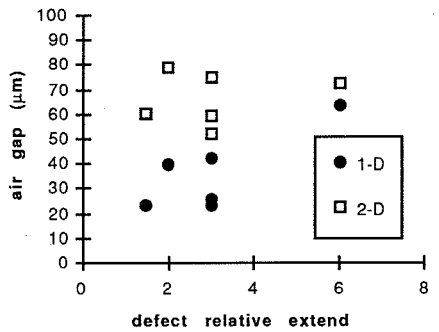

Fig. 7. - Comparison between the resistances (equivalent air gap thickness) obtained through the 1-D and the 2-D inversion procedures vs. d^*

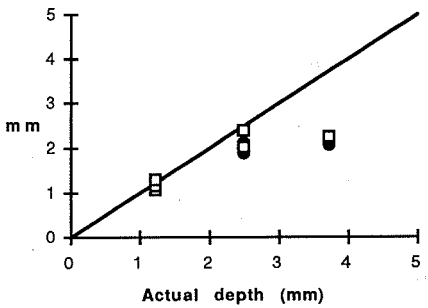

Fig. 8. - Comparison between the inferred defects depths